The Addition of Hydrogen Atoms to Diacetylene and the Heats of Formation of *i*-C_4H_3 and *n*-C_4H_3

Stephen J. Klippenstein* and James A. Miller*

Combustion Research Facility, Sandia National Laboratories, Livermore, California 94551-0969

Received: January 13, 2005; In Final Form: March 11, 2005

In this article, we discuss in detail the addition of hydrogen atoms to diacetylene and the reverse dissociation reactions, $H + C_4H_2 \leftrightarrows i\text{-}C_4H_3$ (R1) and $H + C_4H_2 \leftrightarrows n\text{-}C_4H_3$ (R2). The theory utilizes high-level electronic structure methodology to characterize the potential energy surface, Rice−Ramsperger−Kassel−Marcus (RRKM) theory to calculate microcanonical/*J*-resolved rate coefficients, and a two-dimensional master-equation approach to extract phenomenological (thermal) rate coefficients. Comparison is made with experimental results where they are available. The rate coefficients $k_1(T, p)$ and $k_2(T, p)$ are cast in forms that can be used in chemical kinetic modeling. In addition, we predict values of the heats of formation of *i*-C_4H_3 and *n*-C_4H_3 and discuss their importance in flame chemistry. Our basis-set extrapolated, quadratic-configuration-interaction with single and double excitations (and triple excitations added perturbatively), QCISD(T), predictions of these heats of formation at 298 K are 130.8 kcal/mol for *n*-C_4H_3 and 119.3 kcal/mol for the *i*-isomer; multireference CI calculations with a nine-electron, nine-orbital, complete-active-space (CAS) reference wavefunction give just slightly larger values for these parameters. Our results are in good agreement with the recent focal-point analysis of Wheeler et al. **(***J. Chem. Phys.* **2004**, *121,* 8800−8813), but they differ substantially for ΔH^0_{f298}(*n*-C_4H_3) with the earlier diffusion Monte Carlo predictions of Krokidis et al. (*Int. J. Chem. Kinet.* **2001**, *33,* 808−820).

Introduction

Small unsaturated hydrocarbon free radicals, particularly resonantly stabilized ones, are critical elements of the gas-phase chemistry that ultimately leads to soot formation in rich flames.[1−3] When such radicals can dissociate into another radical and a *stable molecule* (e.g., *n*-C_4H_3, *i*-C_4H_3, *n*- and *i*-C_4H_5, and allyl (C_3H_5) all dissociate in this way), the bond energies are typically small, and the corresponding dissociation rate coefficients can be large. For these radicals, thermal dissociation is an important, perhaps dominant, removal step under combustion conditions. Consequently, for the purposes of modeling and analyzing flames mechanistically, it is crucial to have accurate rate coefficients for the thermal dissociation of such radicals, information that is difficult to obtain directly in the laboratory. Most commonly, such reactions are studied in the reverse radical + molecule direction at low temperature ($T < 900$ K), usually over a narrow range of pressures. From this information, one must infer dissociation rate coefficients at high temperature (there is always an equilibrium shift at some temperature, typically at $T \approx 1000$ K) for a wide range of pressures. Such inferences require very sophisticated, accurate theoretical methods for predicting rate coefficients and thermochemistry. Fortunately, such methods now exist.[4−6] In the present article, we apply them to the two reactions,

$$H + C_4H_2 \leftrightarrows i\text{-}C_4H_3 \qquad \text{(R1)}$$

and

$$H + C_4H_2 \leftrightarrows n\text{-}C_4H_3, \qquad \text{(R2)}$$

and provide rate coefficients that can be used with some confidence in chemical kinetic modeling.

Another motivation for the present work is the assertion made by Wang and Frenklach[7] that "the contribution of the reaction between *n*-C_4H_3 and C_2H_2 to benzene production may be as significant as the propargyl recombination". This conclusion differs markedly from the conclusion drawn earlier by Miller and Melius[8] and is based on modeling three rich flames: two low-pressure acetylene flames and an atmospheric-pressure ethylene flame. However, it was only their modeling of one of these flames, the 20-Torr $C_2H_2/O_2/Ar$ flame studied experimentally by Westmoreland,[9] that appeared to warrant such a conclusion. In their flame calculations, there exists a "low-temperature" mechanism forming phenyl, i.e.

$$H + C_4H_2 \leftrightarrows n\text{-}C_4H_3 \qquad \text{(R2)}$$

$$n\text{-}C_4H_3 + C_2H_2 \leftrightarrows C_6H_5 \text{ (phenyl)}, \qquad \text{(R3)}$$

which subsequently leads to benzene (C_6H_6) through H-atom addition to phenyl. This process is able to compete favorably in their modeling with propargyl (C_3H_3) recombination, which occurs primarily in the high-temperature regions of the flame. The success of the Wang−Frenklach low-temperature mechanism in competing with propargyl recombination hinges on four different points:

1. The rate coefficient k_2 of reaction R2.
2. The heat of formation (more correctly, the bond energy) of *n*-C_4H_3.
3. The rate coefficient of reaction R3.
4. The rate coefficient for propargyl recombination.

Note that the heat of formation of *n*-C_4H_3 plays a role in the modeling both directly (through the density of states) in determining k_2 and indirectly (through the equilibrium constant of R2) in establishing how much *n*-C_4H_3 can accumulate before

10.1021/jp058017x CCC: $30.25
Published on Web 04/21/2005

R2 equilibrates. Although some confusion apparently exists on this point,[10] the heat of formation of i-C_4H_3 is inconsequential for the issue at hand. Nevertheless, we discuss the theoretical predictions of ΔH^0_{f298} for both isomers and their impact on flame modeling in the analysis below, along with the other three points listed above.

Theoretical Methods

The geometric structures and vibrational frequencies for diacetylene (CHCCCH), i-C_4H_3 (CH_2CCCH), n-C_4H_3 (CHCCHCH), the transition states for adding an H atom to either the central or terminal carbon atoms of diacetylene, and those for isomerizing from i-C_4H_3 to n-C_4H_3 were obtained via density functional theory employing the Becke−3 Lee−Yang−Parr (B3LYP) functional[11] and the 6-311++G(d,p) basis set.[12] For n-C_4H_3, both cis (E-) and trans (Z-) orientations of the terminal HCCH group were considered, along with the planar saddle point connecting these two isomers. The intrinsic reaction path for the addition transition states, and the projected vibrational frequencies along those paths, were also examined at the B3LYP/6-311++G(d,p) level. For the doublet species, unrestricted spin wavefunctions were employed in the present B3LYP calculations, while restricted spin wavefunctions were employed for the singlets.

Higher-level energies were obtained at each of these stationary points, and at each point along the reaction path from spin-restricted, quadratic configuration interaction calculations with perturbative inclusion of the triplet contribution,[13,14] QCISD(T). These QCISD(T) calculations employed the correlation-consistent, polarized-valence, triple-ζ (cc-pvtz) and quadruple-ζ (cc-pvqz) basis sets[15] and were extrapolated to the infinite basis-set limit via the expression[16,17]

$$E[\mathrm{QCISD(T)}/\infty] \approx E[\mathrm{QCISD(T)/cc\text{-}pvqz}] + \{E[\mathrm{QCISD(T)/cc\text{-}pvqz}] - E[\mathrm{QCISD(T)/cc\text{-}pvtz}]\} \times 0.6938 \quad (1)$$

These energies were converted to heats of formation via comparison with related calculations and experimental results for CH_4 and H_2. The B3LYP/6-311++G(d,p) vibrational frequencies were employed in making zero-point energy corrections.

The heats of formation for i- and n-C_4H_3 have been the subject of considerable debate, with a variety of quantum chemical estimates provided in the literature (see, e.g., refs 8, 18−22, and references therein). The presence of large-scale spin contamination in the unrestricted Hartree−Fock wavefunctions for these species ((average spin)^2 = 1.44 and 1.21 for i- and n-C_4H_3, respectively) indicates significant multireference character to their wavefunctions. Furthermore, the somewhat large T1 diagnostic for i-C_4H_3 (0.021) causes some concern regarding the accuracy of coupled-cluster calculations (i.e., QCISD(T) and CCSD(T)) for this species.

To explore this issue, we have performed a multireference configuration interaction (MRCI) analysis of the CH bond strengths in i- and n-C_4H_3. Two different complete active space (CAS), self-consistent field (SCF) reference wavefunctions were employed in these internally contracted MRCI calculations. First, a five-electron, five-orbital (5e,5o) CAS space was considered with the energies evaluated for both the cc-pvtz and cc-pvqz basis sets, followed by an extrapolation to the infinite basis-set limit according to eq 1. Then, the energies were evaluated for a nine-electron, nine-orbital (9e,9o) CAS space employing only the cc-pvtz basis set. The final energy was estimated as the sum of the (5e,5o) infinite basis-set energies and the difference between the (9e,9o) and (5e,5o) cc-pvtz energies. The five orbitals in the (5e,5o) CAS consisted of the in-plane radical p and π,π^* orbitals and the CH σ,σ^* pair for the dissociating CH bond. The (9e,9o) CAS space added the out-of-plane π,π^* orbitals to the (5e,5o) CAS space. All single and double excitations from these reference CASSCF wavefunctions were included, except for the core orbitals, and the Davidson correction for higher-order excitations was evaluated. These calculations were performed in C_s symmetry, even for i-C_4H_3, to maintain a distinction in the CH bonds. The B3LYP/6-311++G(d,p) geometries were used in these MRCI calculations and the CH bond strengths were evaluated from supermolecule calculations in which the dissociating H was held 10 Å away from the diacetylene fragment.

The *MOLPRO* quantum chemistry package[23] was used in the QCISD(T) and MRCI evaluations, which were performed on a Parallel Quantum Solutions linux cluster.[24] The *Gaussian 98* quantum chemistry software was employed in the density functional calculations.[25]

TABLE 1: Heats of Formation for Stationary Points on the C_4H_3 Potential Energy Surface

species	ΔH^0_f (0 K) (kcal/mol)[a]	T1 diagnostic
CHCCCH	110.2	0.014
H	51.7	0
CHCCCH + H	161.9	
i-C_4H_3	119.1	0.021
n-C_4H_3; HCCH cis	131.2	0.015
n-C_4H_3; HCCH trans	131.3	0.015
CHCCCH + H ↔ i-C_4H_3	164.1	0.015
CHCCCH + H ↔ n-C_4H_3	168.7	0.017
n-C_4H_3; HCCH cis ↔ n-C_4H_3; HCCH trans	135.4	0.015
i-C_4H_3 ↔ n-C_4H_3	173.0	0.019

[a] From QCISD(T)/cc-pvtz//B3LYP/6-311++G(d,p) and QCISD(T)/cc-pvqz//B3LYP/6-311++G(d,p) calculations extrapolated to the infinite basis-set limit. B3LYP/6-311++G(d,p) zero-point corrections are included.

The present QCISD(T)-calculated heats of formation for the key stationary points on the C_4H_3 potential energy surface are provided in Table 1. The B3LYP/6-311++G(d,p) geometries, rotational constants, and vibrational frequencies for these stationary points are reported in the Supporting Information. The isomerization barrier from i-C_4H_3 to n-C_4H_3 (via a 1,2 H transfer) of 53.9 kcal/mol lies higher in energy than either of the barriers to dissociation. Furthermore, the isomerization transition state is much tighter, with a lower entropy, than the addition/dissociation transition states. Thus, the isomerization between the two addition complexes is insignificant, and the two addition reactions may be treated separately. Efforts to locate a 1,3 H-transfer saddlepoint were unsuccessful, yielding instead geometries that correspond effectively to the loss of the H atom. Similarly, isomerizations through a CH_2CHCC radical were found to lie too high in energy to be relevant to either the addition kinetics of CHCCCH + H or the dissociation kinetics of the C_4H_3 species.

In contrast, the isomerization between the cis (E-) and trans (Z-) forms of n-C_4H_3 involves only a 4.2 kcal/mol barrier, implying that the two species are rapidly equilibrated at energies near the dissociation threshold. The vibrational frequencies of the E and Z forms are very similar (differing by 5% or less), and the energetic splitting between the two is very small (0.09 kcal/mol). Thus, it seems reasonable to treat the addition to form n-C_4H_3 as a single-well problem with a density of states given by twice that for the E form. A more accurate treatment, which

TABLE 2: CH Bond Dissociation Energies (kcal/mol)

species	QCISD(T)[a]	MRCI (5e,5o)[b]	MRCI (9e,9o)[c]	MRCI (9e,9o)/∞[d]	MRCI + Q (5e,5o)[e]	MRCI + Q (9e,9o)[f]	MRCI + Q (9e,9o)/∞[g]
i-C_4H_3	42.7	38.6	37.2	37.2	40.9	41.2	41.3
(*E*)-*n*-C_4H_3	30.7	28.8	26.9	26.8	31.1	29.7	29.6
difference	12.0	9.8	10.3	10.4	9.8	11.5	11.7

[a] QCISD(T)/cc-pvtz and QCISD(T)/cc-pvqz calculations extrapolated to the infinite basis-set limit. All calculations include B3LYP/6-311++G(d,p) evaluated zero-point corrections. [b] MRCI/cc-pvtz and MRCI/cc-pvqz calculations employing a (5e,5o) CASSCF reference wavefunction and extrapolated to the infinite basis-set limit. [c] MRCI/cc-pvtz calculations employing a (9e,9o) CASSCF reference wave function. [d] Approximate basis-set extrapolated (9e,9o) MRCI calculations obtained from the sum of extrapolated (5e,5o) calculations, and the difference between (9e,9o) and (5e,5o) MRCI calculations employing the cc-pvtz basis set. [e] As in footnote b, but including the Davidson correction. [f] As in footnote c, but including the Davidson correction. [g] As in footnote d, but including the Davidson correction.

TABLE 3: C_4H_3 Heats of Formation at 0 K (kcal/mol)

method	*i*-C_4H_3	(*E*)-*n*-C_4H_3	difference
BAC-MP4[a]	111.3	130.9	19.6
DMC[b]	119.1	125.7	6.6
G3[c]	120.1	130.2	11.1
MRCI + Q[d]	120.5	132.3	11.7
QCISD(T)[e]	119.1	131.2	12.0
focal point[f]	119.0	130.8	11.8

[a] Bond addivitity corrected MP4 calculations from ref 8. [b] Diffusion Monte Carlo calculations from ref 21. The present B3LYP/6-311++G(d,p) thermal and zero-point energies are used to convert from 298 to 0 K. [c] As in footnote b, but for G3 calculations rather than diffusion Monte Carlo. [d] Present Davidson corrected approximate infinite basis-set MRCI result for a (9e,9o) CAS reference wavefunction. These predictions are also based on the basis-set extrapolated QCISD(T) numbers for the H and CHCCCH heats of formation. [e] Present basis-set extrapolated QCISD(T) calculations. [f] Focal-point analysis from ref 22.

would consider the anharmonicities in the HCC bending angle and the coupling of the HCC bending mode with the remaining normal modes, was deemed beyond the scope of this work.

The CH distances in the B3LYP saddlepoints to form *i*-C_4H_3 and *n*-C_4H_3 are 2.204 and 1.881 Å, respectively. The determination of the basis-set extrapolated QCISD(T) energies along the addition reaction paths yields maxima at CH separations of 1.939 and 1.768 Å, respectively. The predicted addition barriers along the reaction path are then increased by 1.2 kcal/mol for *i*-C_4H_3 and by 0.5 kcal/mol for *n*-C_4H_3, relative to the values at the B3LYP/6-311++G(d,p) saddlepoints.

The present QCISD(T) and MRCI predictions for the CH bond dissociation energies in *i*-C_4H_3 and *n*-C_4H_3 are presented in Table 2. The QCISD(T) results are seen to agree with the Davidson-corrected MRCI results to within 2 kcal/mol, with the best MRCI + Q results differing by only 1.4 and 1.1 kcal/mol for the *i*- and *n*-C_4H_3 bond dissociation energies, respectively. Notably, the discrepancy in the relative bond dissociation energy is much smaller, only 0.3 kcal/mol. The uncorrected MRCI results significantly underpredict the bond dissociation energies. The relatively large size of the Davidson correction (i.e., as much as 4.1 kcal/mol) suggests that the present QCISD(T) estimates are likely to be just as accurate as the Davidson-corrected MRCI results. Thus, the kinetic estimates presented below are based on the QCISD(T) predictions.

The present predictions of the heats of formation for the *i*- and *n*-C_4H_3 radicals are compared with selected literature values[8,18−22] in Table 3. The detailed CCSD(T)-based focal-point analysis of Wheeler et al.,[22] which appeared while this manuscript was in preparation, should provide the most accurate estimates to date. The present QCISD(T) values are in excellent agreement with this focal-point analysis. This good agreement suggests that the present method should also provide accurate energies for the other stationary points of importance to the present kinetic analysis. The discrepancy with the diffusion

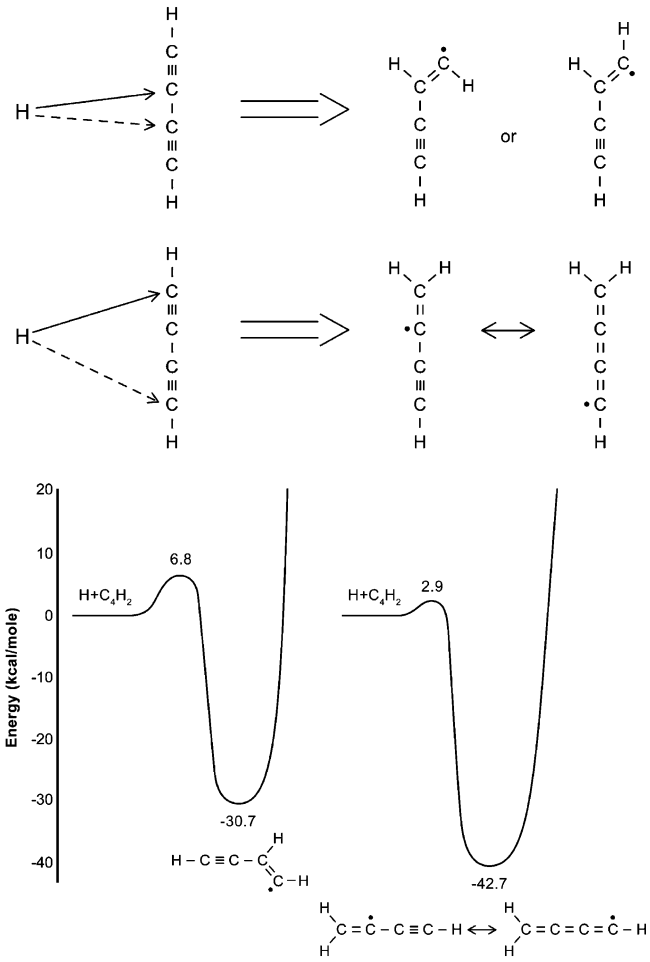

Figure 1. (a) Diagram showing the attack by hydrogen atoms on the central and terminal carbon atoms in diacetylene and the structures of the radicals produced. (b) Potential energy diagrams for the formation of *n*-C_4H_3 and *i*-C_4H_3.

Monte Carlo estimates almost certainly indicates a limitation in the inherent assumptions of that approach, such as the fixed-node approximation. More detailed comparisons of prior literature estimates are provided in ref 22.

From information about the potential energy surface, shown diagrammatically in Figure 1, we determine phenomenological (thermal) rate coefficients by methods identical to those employed in our work on vinyl and ethyl dissociation.[5] Briefly, we calculate microcanonical (*J*-resolved) rate coefficients, $k(E, J)$, from RRKM theory. Both conventional and variational (microcanonical/*J*-resolved) transition-state theory (TST) are used in these calculations. In conventional transition-state theory, the transition-state dividing surface is placed at the saddlepoint separating the reactants from the product and is perpendicular to the minimum-energy path connecting them. In the variational

approach, the dividing surface is chosen from a one-parameter family of surfaces perpendicular to the minimum energy path; there is one dividing surface for every E, J combination, and the minimum-flux condition is used to establish the position of the surface and the corresponding $k(E, J)$. Tunneling and nonclassical reflection are included in the analysis one-dimensionally by assuming that the minimum-energy path can be approximated by an Eckart function. We believe that such a one-dimensional approximation is probably quite accurate for simple bond-breaking/bond-forming reactions, where the reaction path curvature is minimal.

The rate coefficients $k(E, J)$ are used as input into a two-dimensional master equation (ME) in which E, the *total internal energy*, and J, the *total angular momentum* quantum number, are the independent variables (the E, J model of ref 4). For the purpose of comparison, we also utilize a one-dimensional ME in which E is the independent variable (the E model of ref 4). In our analysis, the reaction is assumed to take place in a bath of molecular nitrogen (N_2), and the energy transfer function $P(E, E')$ is assumed to be describable by a single-exponential-down model with $\langle \Delta E_d \rangle = 100(T/300)\ \mathrm{cm}^{-1}$. This expression for $\langle \Delta E_d \rangle$ was estimated from our previous experience with other molecules.[4,5] The specific master equation used in our analysis describes the *irreversible dissociation* of the adduct radicals. The association rate coefficients are determined from detailed balance, which must be satisfied exactly.[6] The dissociation rate coefficients themselves are calculated by a variety of methods based on identifying the rate coefficient with the largest (least negative) eigenvalue of the transition matrix of the master equation.[4]

Although such a possibility is not included in the present analysis, n-C_4H_3 can also dissociate directly into $C_2H + C_2H_2$. This channel is about 28 kcal/mol higher in energy than $H + C_4H_2$. Nevertheless, on the basis of measured values of the $C_2H + C_2H_2 \rightarrow C_4H_2 + H$ rate coefficient, we estimate that the $C_2H + C_2H_2$ channel could account for as much as 20% of the n-C_4H_3 dissociation rate coefficient *in the high-pressure limit* at 2000 K. Of course, this contribution drops dramatically as the pressure (and/or temperature) is reduced, so that for any realistic pressure the $C_2H + C_2H_2$ channel is completely negligible.

The High-Pressure Limit

Figure 2 shows our predictions for $k_{1\infty}$ and $k_{2\infty}$ using the QCISD(T)/∞ potential; the theory incorporates variational effects as discussed above and includes tunneling. Unless stated otherwise, these latter two effects are always included in the results that follow. As one would expect from the relative heights of the two barriers to addition (Figure 1), $k_{1\infty} \gg k_{2\infty}$ at virtually all temperatures of interest. Nava et al.[26] measured the total rate coefficient for $H + C_4H_2$ (i.e., $k_1 + k_2$) in the temperature range $210\ \mathrm{K} \le T \le 423\ \mathrm{K}$ and at pressures ranging from 5 to 300 Torr. They conclude that their rate coefficients are independent of pressure and thus are indicative of the high-pressure limit. We agree. Our predictions of $k_{1\infty}$ and $k_{2\infty}$ using the QCISD(T)/∞ surface are somewhat smaller than the experimental results, but the two can be brought into almost perfect agreement by reducing the barrier height for reaction R1 by $^1/_2$ kcal/mol. To maintain consistency between the two quantum chemical results (we believe there should be no more error in one barrier height than the other), we have also reduced the R2 barrier height by $^1/_2$ kcal/mol. These modified predictions are also shown in Figure 2. The remainder of the analysis in this article utilizes the adjusted barrier heights.

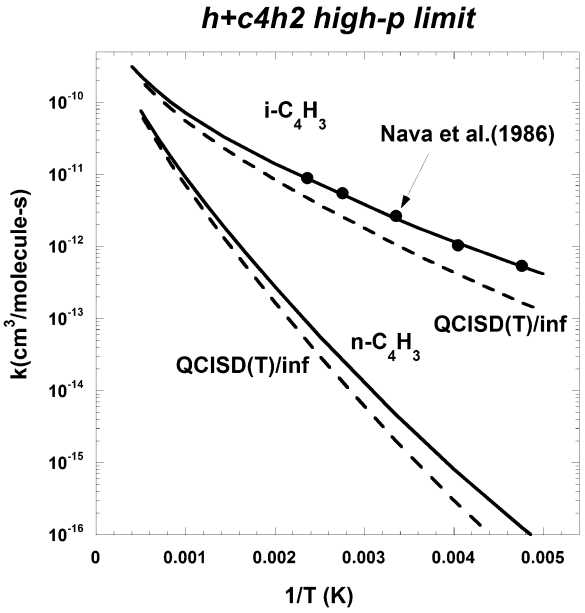

Figure 2. High-pressure-limit calculations of k_1 and k_2 compared with the measurements of Nava et al.[26] Both the predictions with the restricted QCISD(T)/∞ barrier heights and those with these barrier heights adjusted downward by $^1/_2$ kcal/mol are shown.

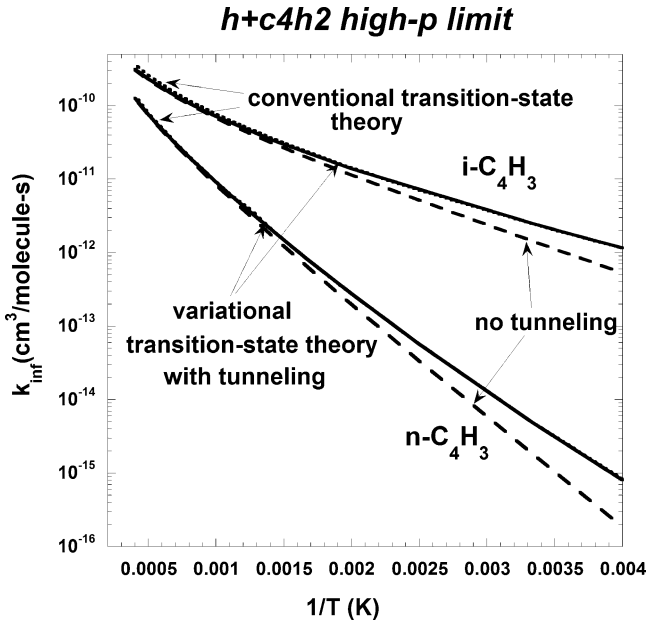

Figure 3. Variational and tunneling effects on $k_{1\infty}(T)$ and $k_{2\infty}(T)$. Our predictions of the high-pressure-limit rate coefficients can be represented well by the expressions $k_{1\infty} = 7.16 \times 10^{-14} T^{1.119} \exp(-1672/RT)$ and $k_{2\infty} = 1.35 \times 10^{-14} T^{1.305} \exp(-5018/RT)$ cm^3/molecule−s, where $R = 1.987$ cal/mol−K.

Figure 3 illustrates the impact of neglecting variational effects and tunneling on both $k_{1\infty}$ and $k_{2\infty}$. As one would expect, for reactions with pronounced potential energy barriers, variational effects are small for both reactions. The maximum effect in both cases is at the highest temperature considered, 2500 K. For $k_{1\infty}$, the conventional TST value at this temperature is larger than the variational result by 15%. For $k_{2\infty}$, the conventional TST rate coefficient is larger by only 7%. Tunneling has a substantial effect on both rate coefficients at low temperature, increasing $k_{1\infty}$ by a factor of 2.2 at 250 K and increasing $k_{2\infty}$ by a factor of 4.4 at the same temperature. Of course, the effect of tunneling decreases as the temperature goes up.

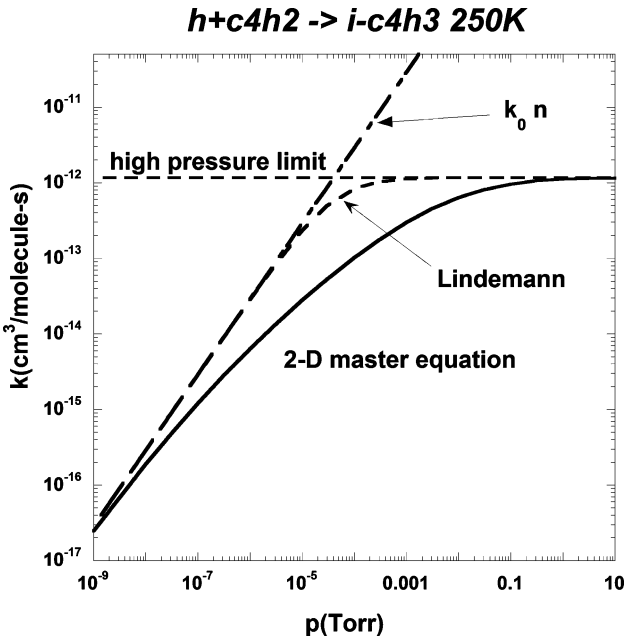

Figure 4. Pressure dependence of $k_1(T, p)$ for R1, H + C_4H_2 ⇆ *i*-C_4H_3, at $T = 250$ K.

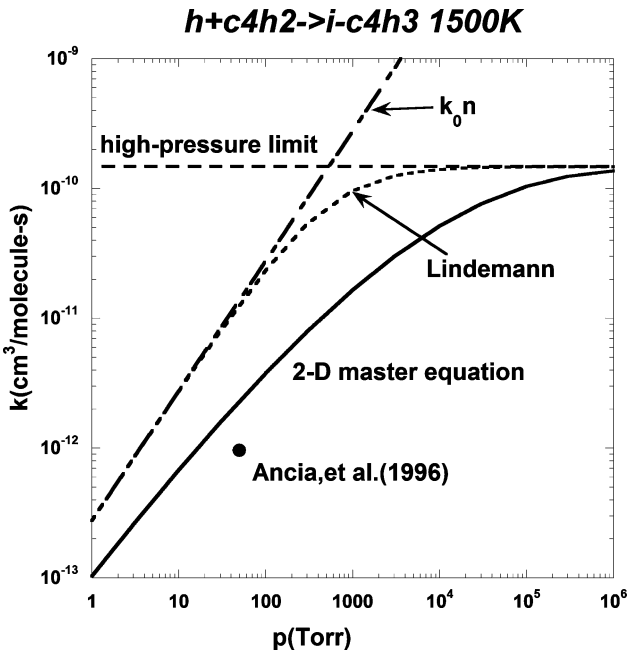

Figure 5. Pressure dependence of $k_1(T, p)$ for R1, H + C_4H_2 ⇆ *i*-C_4H_3, at $T = 1500$ K. Note that the Ancia et al.[34] rate coefficient was actually obtained at $T = 1660$ K (see text).

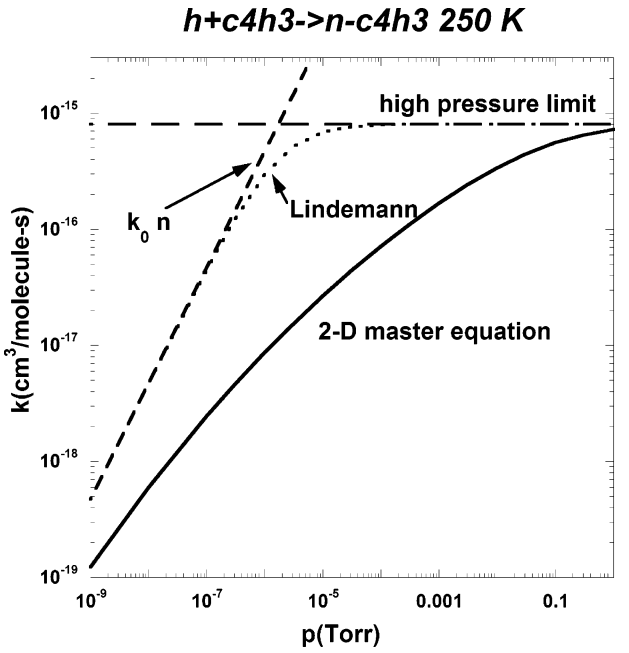

Figure 6. Pressure dependence of $k_2(T, p)$ for R2, H + C_4H_2 ⇆ *n*-C_4H_3, at $T = 250$ K.

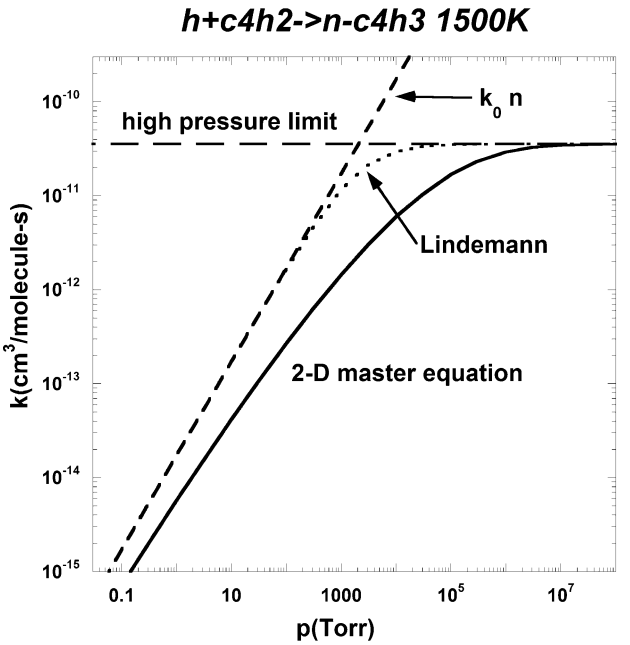

Figure 7. Pressure dependence of $k_2(T, p)$ for R2, H + C_4H_2 ⇆ *n*-C_4H_3, at $T = 1500$ K.

Pressure Dependence

Figures 4 and 5 show the pressure dependence of k_1 predicted theoretically at 250 and 1500 K respectively; Figures 6 and 7 show the same results for k_2. Results for both $k_1(T, p)$ and $k_2(T, p)$ at temperatures of 500, 1000, 2000, and 2500 K are given in the Supporting Information for this article. At most pressures of interest in combustion (roughly 20 Torr to 10 atm), both rate coefficients have their high-pressure limiting values at low temperature, but at high temperatures, both rate coefficients are fairly far removed from both limits. Consequently, it is extremely important to model the pressure dependence of both rate coefficients accurately.

Ideally, one would like to have measurements of k_1 and k_2 (or k_{-1} and k_{-2}) at high temperatures (i.e., away from their high-pressure limits) in order to test the $P(E, E')$ functions used in the analysis (i.e., the values of $\langle \Delta E_d \rangle$ employed). Unfortunately, there is a dearth of such experimental data available. The only measurement we could find is that of Ancia et al.,[33] who measured the H + C_4H_2 total rate coefficient in a 50-Torr ethane flame at $T = 1660$ K. This rate coefficient is shown in Figure 5 even though the experimental and theoretical temperatures are somewhat different. The exact comparison, at 1660 K, is $k_{tot} \equiv k_1 + k_2 = 1.46 \times 10^{-12}$ cm^3/molecule−s from the theory compared with $k_{tot} = 9.61 \times 10^{-13}$ cm^3/molecule−s from the experiment. This represents a discrepancy of about 50%. Ancia et al. do not give error bars for their rate coefficient, but errors of at least a factor of 2 are to be expected from inferring rate coefficients from flame profiles. In any event, one should not take this comparison too seriously. Using measured values

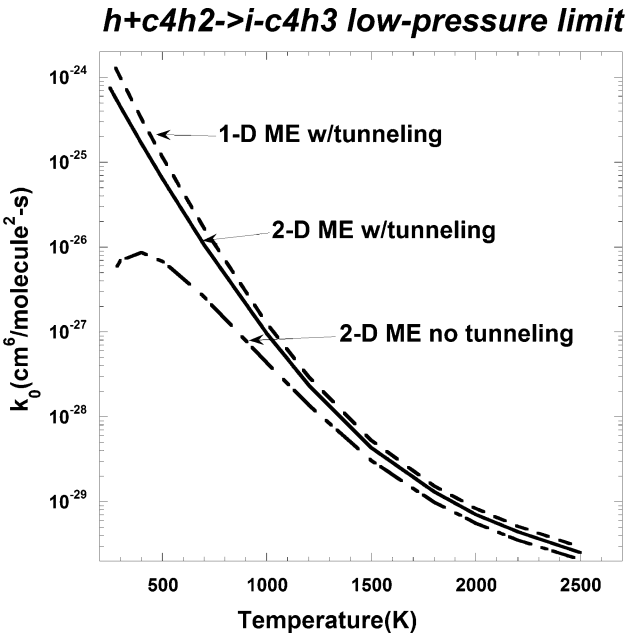

Figure 8. Low-pressure-limit rate coefficient k_{1_0} for reaction R1, H + C_4H_2 ⇆ *i*-C_4H_3.

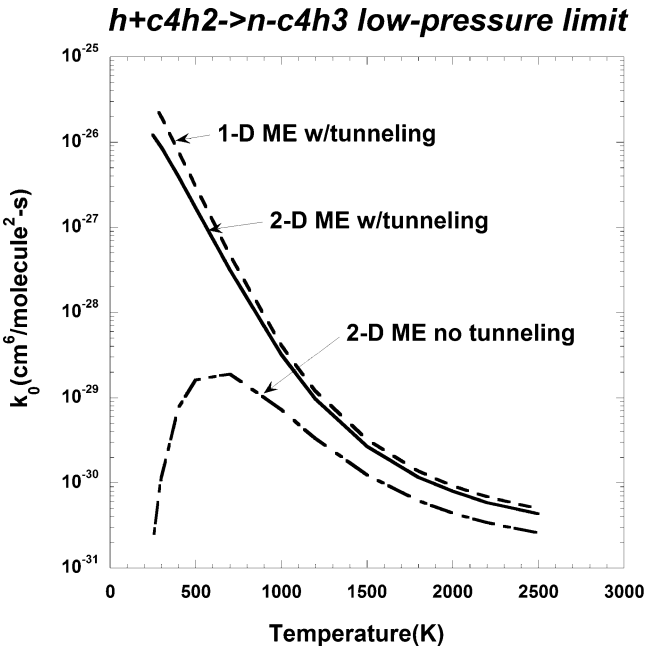

Figure 9. Low-pressure-limit rate coefficient k_{2_0} for reaction R2, H + C_4H_2 ⇆ *n*-C_4H_3.

for the rate coefficient of $C_2H + C_2H_2 \rightarrow C_4H_2 + H$ and its equilibrium constant, one would deduce a value comparable to these numbers for the rate coefficient of the exchange reaction, $H + C_4H_2 \rightarrow C_2H + C_2H_2$, under these conditions. Also, the abstraction (which is ~30 kcal/mol endothermic) cannot be completely ignored. However, the main problem is that one would expect all three reactions (addition, exchange, and abstraction) to be highly equilibrated under the conditions of the flame measurement, with equilibrium probably favoring the reactants. In such a situation, it is not clear how the measurement really should be interpreted.

The Low-Pressure Limit

The low-pressure-limit rate coefficients k_{1_0} and k_{2_0} are plotted in Figures 8 and 9, respectively. In our previous work on C_2H_3 and C_2H_5 dissociation,[5] we pointed out that, for association/dissociation reactions with intrinsic potential energy barriers, the value of the low-pressure-limit rate coefficient is *independent of the existence of the barrier*. However, the low-pressure limit is approached much more slowly with decreasing pressure when a barrier is present than when it is not. This difference occurs because reaction just above "threshold" must take place strictly by tunneling when a barrier is present. This is the situation for both reactions R1 and R2. When tunneling is included in the theory, both k_{1_0} and k_{2_0} are continuously decreasing functions of temperature, as they would be if no barrier were present. However, if we neglect tunneling in the theory, both k_{1_0} and k_{2_0} first increase with temperature before they drop off at high T, as shown in the plots. At $T = 250$ K, tunneling causes an increase in k_{2_0} of almost 5 orders of magnitude. Because of the smaller barrier to association, the increase in k_{1_0} due to tunneling is just slightly more than 2 orders of magnitude. It should be understood that these differences in rate coefficients are strictly due to differences in the threshold energies for dissociation in the two cases (i.e., with and without tunneling), rather than due to any dynamical aspect of tunneling itself. When tunneling is not included, the threshold energy for dissociation is incorrectly assumed to be the bond energy plus the energy barrier, instead of just the bond energy.

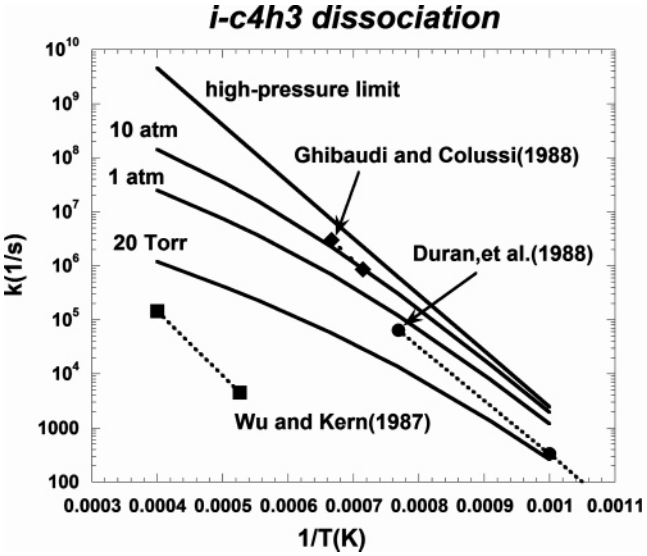

Figure 10. Dissociation rate coefficients $k_{-1}(T, p)$ at various pressures for R1, H + C_4H_2 ⇆ *i*-C_4H_3.

Also displayed in Figures 8 and 9 are the theoretical predictions for k_{1_0} and k_{2_0} when only a one-dimensional (in E) master equation is employed in the analysis. At 250 K, the 1-D ME results are larger than the 2-D predictions by a factor of 2.3 for k_{1_0} and a factor of 2.5 for k_{2_0}. The differences between the 1-D and 2-D predictions become smaller as the temperature increases, as was also the case in our previous work on the dissociations of C_2H_3, C_2H_5, and CH_4.[4−5]

Dissociation Rate Coefficients

In Figure 10, we have plotted our theoretical predictions of $k_{-1}(T, p)$ for a variety of pressures; the same predictions for $k_{-2}(T, p)$ are shown in Figure 11. To our knowledge, there are no measurements of either rate coefficient at any temperature and pressure. However, a number of investigators have estimated

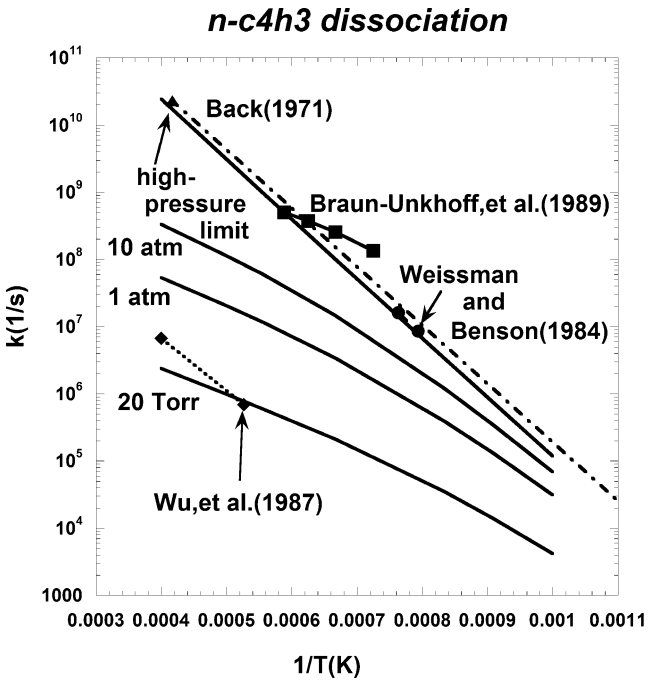

Figure 11. Dissociation rate coefficients $k_{-2}(T, p)$ at various pressures for R2, H + C_4H_2 ⇆ *n*-C_4H_3.

values of $k_{-1}(T, p)$ and $k_{-2}(T, p)$ (using methods of varying degrees of sophistication) for use in modeling or mechanistic analysis. A number of these estimates are shown on the plots. They are included here simply to illustrate the uncertainty that exists in these rate coefficients at high temperature, not to criticize any of the work involved. In fact, the rate coefficients in question may well not have been a significant factor in these prior analyses. These other rate coefficients are generally (but not always) larger that those deduced from the present theory. The Ghibaudi/Colussi[27] estimate of k_{-1} was intended to apply to experiments conducted at $p = 0.5$ atm; it is roughly a factor of 3−4 larger than our prediction at 1 atm. The Durán et al.[28] rate coefficient was applied in modeling at pressures of 0.1 and 1 atm. The estimates by Back[29] and Weissman and Benson[30] indeed are estimates of $k_{-2\infty}(T)$, putting them in good agreement with our theoretical result for this rate coefficient. However, they were intended to apply to experiments at pressures of $p \approx$ 1 atm, resulting in the fairly large discrepancies shown in Figure 11. The rate coefficient of Braun-Unkhoff et al.[31] included falloff effects and was included in modeling of experiments at pressures between 1.5 and 6 atm. Some of the difference between their value of k_{-2} and ours shown in Figure 11 may be attributable to different bath gases, toluene versus molecular nitrogen. However, this cannot account for all the difference, because their rate coefficient is slightly larger than our value of $k_{-2\infty}$, the high-pressure limit. The rate coefficients of Wu et al.[32] were given as second-order processes that we converted to the first-order rate coefficients shown in the figure. They were intended to apply to pressures between 0.3 and 0.6 atm, but they are somewhat smaller than our predictions at these pressures.

The comparisons discussed above illustrate the need for accurate values of $k_{-1}(T, p)$ and $k_{-2}(T, p)$ for use in modeling. We believe the results of this article fill that need, although it certainly would be desirable to have some experiments with which to compare.

Nonequilibrium Factors

The nonequilibrium factor f_{ne} was originally introduced by Smith, McEwan, and Gilbert.[33] It is defined by the expression,

$$f_{ne} = 1/\left[\int_0^\infty \frac{x(E)}{F(E)} x(E)\, dE\right], \quad (2)$$

where $x(E)$ is the steady-state energy distribution of a dissociating molecule during its *irreversible* dissociation, and $F(E)$ is its equilibrium distribution. The two distributions are assumed to be normalized so that

$$\int_0^\infty x(E)\, dE = \int_0^\infty F(E)\, dE = 1. \quad (3)$$

Clearly, the deviation of f_{ne} from unity is a measure of the degree to which dissociation causes $x(E)$ to deviate from equilibrium (note that setting $x(E) = F(E)$ in eq 1 for all energies results in $f_{ne} = 1$). However, f_{ne} is very close to unity unless states that are highly populated at equilibrium have their populations disturbed by reaction (i.e., unless the reaction occurs sufficiently rapidly that it interferes with the vibrational−rotational relaxation process itself[6]). If such an interference occurs, a significant fraction of the reaction takes place during the vibrational−rotational relaxation period. In fact, for an experiment in which the reaction is going in the association direction, $1 - f_{ne}$ is the fraction of the deficient reactant (under pseudo-first-order conditions) that is consumed during the internal-energy relaxation period. It is also the relative contribution to the "long-time" association rate coefficient of the "fast-relaxing" modes of the system (those nominally corresponding to vibrational−rotational relaxation). As we showed in a recent article,[6] even though a large amount of reaction may occur as part of the vibrational−rotational relaxation process, there will always be a period of time, perhaps only late in the reaction but before equilibrium is reached, during which phenomenological rate laws will apply with rate coefficients that satisfy detailed balance. It is these long-time rate coefficients that come out of the theory described above.

The discussion of the last paragraph applies qualitatively whether an experiment is designed to measure the association rate coefficient or that for dissociation. However, the precise interpretation of f_{ne} given applies only to association. Nevertheless, a deviation of f_{ne} from unity means that a substantial amount of reaction occurs during the internal-energy relaxation period of a dissociation experiment as well.

With the introduction above in mind, in Figures 12 and 13, we have plotted values of f_{ne} as a function of temperature at various pressures for *i*-C_4H_3 and *n*-C_4H_3, respectively. In both cases, at low pressures, f_{ne} begins to deviate from unity at temperatures just above 1000 K. At temperatures where reaction is usually the most intense in flames, $T \approx 1500-1600$ K, $f_{ne} >$ 0.8 for any pressure of practical interest. Consequently, the long-time rate coefficients given in this article are probably satisfactory for flame modeling. However, for experiments conducted in shock tubes at very high temperatures (e.g., $T > 2000$ K), this may not be the case, even though we would be hard-pressed to propose a simple alternative.

Representations of the Rate Coefficients for Modeling

The rate coefficients calculated by the methods described above correspond to "long-time" rate coefficients, as described in the last section, and consequently, they satisfy detailed balance. Therefore, we provide here representations of the

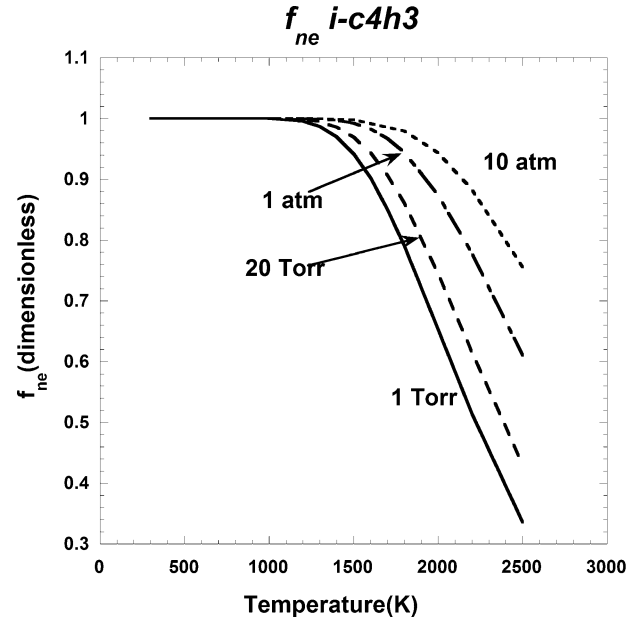

Figure 12. Nonequilibrium factors f_{ne} (defined by eq 2) at various pressures for R1, H + C_4H_2 ⇆ *i*-C_4H_3.

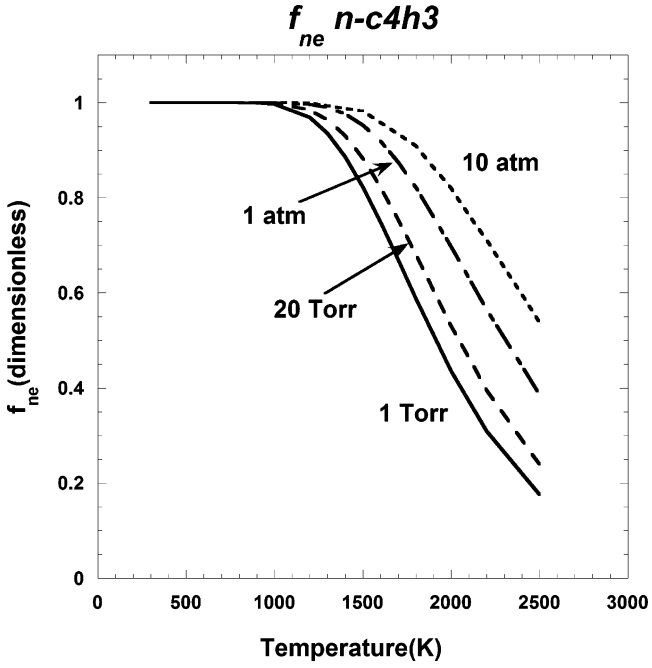

Figure 13. Nonequilibrium factors f_{ne} (defined by eq 2) at various pressures for R2, H + C_4H_2 ⇆ *n*-C_4H_3.

association rate coefficients, $k_1(T, p)$ and $k_2(T, p)$, for use in modeling. The reverse dissociation rate coefficients can then be calculated directly from the detailed balance condition,

$$\frac{k_i(T,p)}{k_{-i}(T,p)} = K_{eq_i}(T), \quad i = 1, 2 \tag{4}$$

where $K_{eq_i}(T)$ is the equilibrium constant for the *i*th reaction.

Rate coefficients for R1, $k_1(T, p)$, can be represented satisfactorily in the Troe format. Least-squares fits to the master-equation results yield the following parameters for 250 K ≤ *T* ≤ 2500 K

$$k_{1\infty} = 7.16 \times 10^{-14} T^{1.158} \exp(-1752.9/RT) \text{ cm}^3/\text{molecule}-\text{s}$$

$$k_{1_0} = 6.34 \times 10^{-3} T^{-8.095} \exp(-2506.6/RT) \text{ cm}^6/\text{molecule}^2-\text{s}$$

and

$$F_c = 0.0748 \exp(2.372 \times 10^{-4} T)$$

where $R = 1.987$ cal/mol−K. Note that this expression for $k_{1\infty}$ is not the same as that given in the caption to Figure 3 above. The expressions in the figure caption are fits only to the limiting rate coefficients; the Troe parameters given here come from fitting all the results.

The rate coefficients for R2, $k_2(T, p)$, cannot be represented satisfactorily in the Troe format. Instead, we give them in the form (Table 4),

$$k_2(T,p) = \sum_{j=1}^{2} A_j(p) T^{n_j} \exp[-E_0^{(j)}(p)/RT], \tag{5}$$

i.e., the rate coefficient at any pressure is represented as a sum of two modified Arrhenius functions. These results can be used directly in *CHEMKIN 4.0*,[35] which interpolates log *k* linearly as a function of log *p* at any temperature to obtain the desired $k(T, p)$. Any number of pressures can be included in the *CHEMKIN* input. Figure 14 displays our calculated rate coefficients for the pressures included in Table 4. The double modified Arrhenius functions (Table 4) represent the master-equation results to better than 6% for 250 K ≤ *T* ≤ 2500 K, with the largest errors occurring at 2500 K.

The Heats of Formation of *i*-C_4H_3 and *n*-C_4H_3 and Their Effects on Cyclization in Rich Flames of Aliphatic Fuels

In their 1992 article,[8] Miller and Melius, in studying benzene formation in rich, low-pressure acetylene flames, concluded that the reactions of *n*-C_4H_3 and *n*-C_4H_5 with acetylene,

$$n\text{-}C_4H_3 + C_2H_2 \leftrightarrows C_6H_5 \tag{R3}$$

and

$$n\text{-}C_4H_5 + C_2H_2 \leftrightarrows C_6H_6 + H, \tag{R4}$$

could not account for the benzene levels observed in such flames, contradicting earlier proposals by Frenklach and co-workers.[36] The reason is that, in such H-atom-rich environments, the *n*-isomers of C_4H_3 and C_4H_5 are relatively easily converted to their more stable *i*-forms by reactions such as

$$n\text{-}C_4H_3 + H \leftrightarrows i\text{-}C_4H_3 + H \tag{R5}$$

and

$$n\text{-}C_4H_5 + H \leftrightarrows i\text{-}C_4H_5 + H. \tag{R6}$$

Actually, the isomeric composition of C_4H_5 was not an issue, because its total concentration in the flame investigated by Miller and Melius was too small for R4 to be a factor, even if all of it was *n*-C_4H_5. A large number of subsequent investigations by other workers have supported the Miller−Melius conclusion.[1]

In a recent article, Frenklach[10] questioned the validity of the Miller−Melius result, stating that "Past numerical analysis[7,37] revealed that Miller and Melius'[s] conclusion on the C_4H_3 and

TABLE 4: Rate Coefficients for R2, H + C_4H_2 → *n*-C_4H_3, in the Form $k_2 = A_1T^{n_1}\exp(-E_0^{(1)}/RT) + A_2T^{n_2}\exp(-E_0^{(2)}/RT)$[a]

pressure	$\log_{10} A_1$	n_1	$E_0^{(1)}$	$\log_{10} A_2$	n_2	$E_0^{(2)}$
20 Torr	39.378	−15.66	24018	8.84	−6.4928	9726.1
90 Torr	33.496	−13.616	22832	6.4263	−5.6133	9389.7
1 atm	26.084	−11.049	21571	2.7606	−4.3335	8703.8
10 atm	17.501	−8.1799	19790	1.2419	−3.7911	8465.8
100 atm	11.988	−6.3292	19322	−3.0373	−2.3188	7603.7

[a] The units of k_2 are cm^3/molecule−s, $R = 1.987$ cal/mol−K.

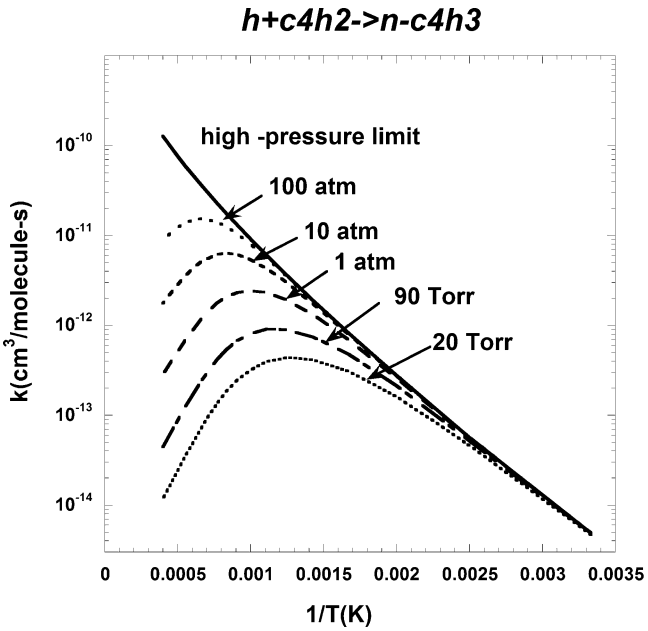

Figure 14. Values of $k_2(T, p)$ as a function of temperature at a number of fixed pressures.

TABLE 5: Heats of Formation at 298 K (in kcal/mol) for *i*-C_4H_3 and *n*-C_4H_3 from Various Methods[a]

	BAC-MP4	DMC	QCISD(T)/∞	MRCI(9e,9o)/∞
n-C_4H_3	129.9	126.0	130.8	131.9
i-C_4H_3	111.3	119.4	119.3	120.8

[a] QCISD(T)/∞ and MRCI(9e,9o)/∞ results are based on a heat of formation for C_4H_2 of 110.8 kcal/mol at 298 K.

C_4H_5 abundances originated primarily from the much lower stabilities predicted by BAC-MP4 for the *n*-forms relative to the corresponding *iso*-forms of these radicals, which is especially pronounced in the case of the C_4H_3 isomers". Of course, the reason that the heats of formation are an issue is that reactions R5 and R6 tend toward establishing equilibrium between the two isomeric forms of the radicals, and the difference between the heats of formation of the two different isomers plays a major role in determining the equilibrated concentrations. Frenklach goes on to discuss the DMC (diffusion Monte Carlo) prediction of the heats of formation of the C_4H_3 and C_4H_5 isomers made by Lester and co-workers,[21] emphasizing that these are quite different from the BAC-MP4 predictions, but similar to the values he has consistently used in his modeling. In the latter, there is a difference of ∼8 kcal/mol between the heats of formation of the two C_4H_3 isomers. For convenience, we show all the theoretical heats of formation at 298 K for the C_4H_3 isomers in Table 5, including the present QCISD(T) and MRCI results. Frenklach concludes by stating that "The higher stability of *n*-C_4H_3 and *n*-C_4H_5 predicted by DMC 'restores' the importance of reactions R3 and R4 [our numbering]."

Of the two references cited by Frenklach in the first quotation above, one is the Wang−Frenklach paper mentioned in the Introduction, and the other only mentions the heat-of-formation issue in passing. Neither actually argues that the *difference* between the ΔH^0_{f298} values for *n*- and *i*-C_4H_3 is a problem. Moreover, Miller and Melius settled this question in their original paper. One of the points of concern in their analysis was that the multireference character of the *i*-C_4H_3 wavefunction was not captured adequately by the BAC-MP4 method. To see if this factor could alter their conclusion, they considered a test case in which ΔH^0_{f298} (*i*-C_4H_3) was changed to result in a difference of ∼8 kcal/mol in the heats of formation of the two isomers. For the result, we quote their article, "Reactions R3 and R4 [present numbering] are never able to produce enough benzene in our model, even if k_3 and k_4 [again our numbering] are multiplied by 10 (resulting in unreasonably high values), and even if ΔH^0_f (298 K) for *i*-C_4H_3 is raised to 121.7 kcal/mol". The latter number reflects the 8 kcal/mol difference in the heats of formation of the two isomers mentioned above. The bottom line is that Frenklach's criticism of the Miller−Melius analysis is totally without foundation.

The issue brought up by Wang and Frenklach[7] is another matter altogether. At most, it involves the heat of formation of *n*-C_4H_3 (i.e., its bond energy). However, other factors are more important. First and foremost is the rate coefficient for $C_3H_3 + C_3H_3$ recombination,

$$C_3H_3 + C_3H_3 \rightarrow \text{products.} \qquad \text{(R7)}$$

Wang and Frenklach used a value of $k_7 = 1.66 \times 10^{-13}$ cm^3/molecule−s, independent of temperature, in modeling the 20-Torr flame mentioned in the Introduction. Our analysis[38] of reaction R7 indicates that this rate coefficient is about a factor of 20−30 too small at 1600 K, the temperature at the center of the high-temperature reaction zone in the 20-Torr flame. Recent experiments[39−41] indicate that our values of $k_7(T)$ are slightly large. By modifying the potential that governs the $C_3H_3 + C_3H_3$ complex formation so that $k_{7\infty}$ decreases with temperature (rather than increases), we have constructed a model that reproduces all the new measurements of $k_7(T, p)$.[42] The Wang−Frenklach rate coefficient is still an order of magnitude smaller than the predictions of this model at 1600 K for a pressure of 20 Torr. Our own modeling[42] of the 20-Torr flame indicates that correcting the Wang−Frenklach mechanism for k_7 alone is more than sufficient to change their conclusion.

The discussion of the last paragraph notwithstanding, it is worthwhile to consider the other points mentioned in the Introduction. Figure 15 shows our rate coefficients for R2, $k_2(T, p)$, and those used by Wang and Frenklach at pressures of 20 and 90 Torr. At $T = 700$ K, the temperature in the 20-Torr flame where the low-temperature cyclization mechanism (the R2−R3 sequence) is most intense, our values of k_2 are about a factor of 5 smaller than those used by Wang and Frenklach. Making this correction in the Wang−Frenklach mechanism even further reduces the importance of R3 as a cyclization step in the flame. Interestingly (and surprisingly), the values of k_3 that we predict[43] at low temperature are very similar to those used in the modeling of both Miller and Melius and Wang and Frenklach; so, this rate coefficient is not an issue.

The heats of formation given in Table 5, taking due account of the small difference in $\Delta H^0_{f298}(C_4H_2)$ between what we have used in our analysis and that used by Wang and Frenklach in their flame modeling, result in a difference between the DMC bond energy of *n*-C_4H_3 and those from our analysis of more

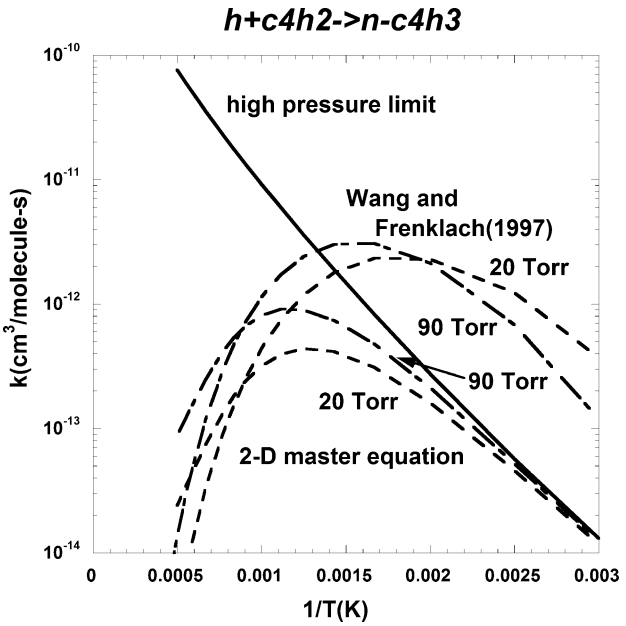

Figure 15. Comparison of the present predictions of $k_2(T, p)$ with those used by Wang and Frenklach[7] at pressures of 20 and 90 Torr.

than 5 kcal/mol. If we increase the n-C_4H_3 bond energy by 5 kcal/mol in our calculation of $k_2(T, p)$, its value at 20 Torr and 700 K is increased by less than 60%. Although not trivial, this difference is not overwhelming. The most important effect of $\Delta H^0_{f298}(n\text{-}C_4H_3)$ is on the equilibrium constant for R2, which determines how much n-C_4H_3 can be formed from that reaction before it equilibrates. This effect is particularly important in flames, where the equilibrium of R2 is likely to shift to favor the reactants at temperatures around 1000 K (of course, the precise temperature depends on $\Delta H^0_{f298}(n\text{-}C_4H_3)$, among other factors). In any event, we find in our modeling that the value of $\Delta H^0_{f298}(n\text{-}C_4H_3)$ used is not an overriding consideration unless the corrections to the Wang−Frenklach mechanism discussed above are not made. We should repeat the point made earlier in this article that the DMC heats of formation are almost certainly flawed, probably because of the "fixed-node" approximation inherent in the approach. By contrast, our QCISD-(T) and MRCI results are in good agreement with the focal-point analysis of Wheeler et al.[22] and are to be preferred.

Concluding Remarks

Our purpose in this article was to provide reliable kinetic information for the reactions,

$$H + C_4H_2 \leftrightarrows i\text{-}C_4H_3 \qquad \text{(R1)}$$

and

$$H + C_4H_2 \leftrightarrows n\text{-}C_4H_3, \qquad \text{(R2)}$$

and good thermochemistry for the i-C_4H_3 and n-C_4H_3 radicals. We believe we accomplished that goal. Our rate coefficient predictions are in good agreement with the very limited amount of experimental information available. Moreover, one should be able to use our results for $k_1(T, p)$ and $k_2(T, p)$, in tandem with the heats of formation provided for i- and n-C_4H_3 ,with some degree of confidence in flame modeling.

Acknowledgment. This work was supported by the United States Department of Energy, Office of Basic Energy Sciences, Division of Chemical Sciences, Geosciences, and Biosciences. Sandia is a multiprogram laboratory operated by Sandia Corporation, a Lockheed-Martin Company, for the United States Department of Energy's National Nuclear Security Administration under contract DE-AC04-94AL85000.

Supporting Information Available: Structural information for the stationary points used in the rate coefficient calculations and falloff curves for additional temperatures are included. This material is available free of charge via the Internet at http://pubs.acs.org.

References and Notes

(1) Miller, J. A.; Pilling, M. J.; Troe, J. *Proc. Combust. Inst.* **2005**, *30*, 43−88.
(2) Miller, J. A. *Faraday Discuss.* **2001**, *119*, 461−475.
(3) Miller, J. A. *Proc. Combust. Inst.* **1996**, *26*, 461−480.
(4) Miller, J. A.; Klippenstein, S. J.; Raffy, C. *J. Phys. Chem. A* **2002**, *106*, 4904−4913.
(5) Miller, J. A.; Klippenstein, S. J. *Phys. Chem. Chem. Phys.* **2004**, *6*, 1192−1202.
(6) Miller, J. A.; Klippenstein, S. J. *J. Phys. Chem. A* **2004**, *108*, 8296−8306.
(7) Wang, H.; Frenklach, M. *Combust. Flame* **1997**, *110*, 173−221.
(8) Miller, J. A.; Melius, C. F. *Combust. Flame* **1992**, *91*, 21−39.
(9) Westmoreland, P. R. Experimental and Theoretical Analysis of Oxidation and Growth Chemistry in a Fuel-Rich Acetylene Flame. Ph.D. Dissertation, Department of Chemical Engineering, Massachusetts Institute of Technology, 1986.
(10) Frenklach, M. *Phys. Chem. Chem. Phys.* **2002**, *4*, 2028−2037.
(11) Becke, A. D. *J. Chem. Phys.* **1993**, *98*, 5648.
(12) Hehre, W. J.; Radom, L.; Pople, J. A.; Schleyer, P. v. R. *Ab Initio Molecular Orbital Theory*; Wiley: New York, 1987.
(13) Curtiss, L. A.; Raghavachari, K.; Redfern, P. C.; Rassolov, V.; Pople, J. A. *J. Chem. Phys.* **1998**, *109*, 7764.
(14) Hampel, C.; Peterson, K.; Werner, H.-J. *Chem. Phys. Lett.* **1992**, *190*, 1.
(15) Dunning, T. H. *J. Chem. Phys.* **1989**, *90*, 1007.
(16) Martin, J. M. L. *Chem. Phys. Lett.* **1996**, *259*, 669.
(17) Feller, D.; Dixon, D. A. *J. Chem. Phys.* **2001**, *115*, 3484.
(18) Cioslowski, J.; Liu, G.; Moncrieff, D. *J. Phys. Chem. A* **1999**, *103*, 11465−11468.
(19) Ceursters, B.; Nguyen, H. M. T.; Peeters, J.; Nguyen, M. T. *Chem. Phys.* **2000**, *262*, 243.
(20) Le, T. N.; Mebel, A. M.; Kaiser, R. I. *J. Comput. Chem.* **2001**, *22*, 1522.
(21) Krokidis, X.; Moriarty, N. W.; Lester, W. A.; Frenklach, M. *Int. J. Chem. Kinet.* **2001**, *33*, 808−820.
(22) Wheeler, S. E.; Allen, W. D.; Schaefer, H. F. *J. Chem. Phys.* **2004**, *121*, 8800−8813.
(23) Amos, R. D.; Bernhardsson, A.; Berning, A.; Celani, P.; Cooper, D. L.; Deegan, M. J. O.; Dobbyn, A. J.; Eckert, F.; Hampel, C.; Hetzer, G.; Knowles, P. J.; Korona, T.; Lindh, R.; Lloyd, A. W.; McNicholas, S. J.; Manby, F. R.; Meyer, W.; Mura, M. E.; Nicklass, A.; Palmieri, P.; Pitzer, R.; Rauhut, G.; Schutz, M.; Schumann, U.; Stoll, H.; Stone, A. J.; Tarroni, R.; Thorsteinsson, T.; Werner, H.-J. *MOLPRO*, version 2002.1.
(24) Parallel Quantum Station QS160-2000R; Parallel Quantum Solutions, 2013 Green Acres Road Suite A, Fayetteville, AR.
(25) Frisch, M. J.; Trucks, G. W.; Schlegel, H. B.; Scuseria, G. E.; Robb, M. A.; Cheeseman, J. R.; Zakrzewski, V. G.; Montgomery, J. A., Jr.; Stratmann, R. E.; Burant, J. C.; Dapprich, S.; Millam, J. M.; Daniels, A. D.; Kudin, K. N.; Strain, M. C.; Farkas, O.; Tomasi, J.; Barone, V.; Cossi, M.; Cammi, R.; Mennucci, B.; Pomelli, C.; Adamo, C.; Clifford, S.; Ochterski, J.; Petersson, G. A.; Ayala, P. Y.; Cui, Q.; Morokuma, K.; Malick, D. K.; Rabuck, A. D.; Raghavachari, K.; Foresman, J. B.; Cioslowski, J.; Ortiz, J. V.; Stefanov, B. B.; Liu, G.; Liashenko, A.; Piskorz, P.; Komaromi, I.; Gomperts, R.; Martin, R. L.; Fox, D. J.; Keith, T.; Al-Laham, M. A.; Peng, C. Y.; Nanayakkara, A.; Gonzalez, C.; Challacombe, M.; Gill, P. M. W.; Johnson, B. G.; Chen, W.; Wong, M. W.; Andres, J. L.; Head-Gordon, M.; Replogle, E. S.; Pople, J. A. *Gaussian 98*; Gaussian, Inc.: Pittsburgh, PA, 1998.
(26) Nava, D. P.; Mitchell, M. B.; Stief, L. J. *J. Geophys. Res.* **1986**, *91*, 4585−4589.
(27) Ghibaudi, E.; Colussi, A. J. *J. Phys. Chem.* **1988**, *92*, 5839−5842.
(28) Durán, R. P.; Amorebieta, V. T.; Colussi, A. J. *J. Phys. Chem.* **1988**, *92*, 636−640.
(29) Back, M. H. *Can. J. Chem.* **1971**, *49*, 2199.
(30) Weissmann, M.; Benson, S. W. *Int. J. Chem. Kinet.* **1984**, *16*, 307−333.

(31) Braun-Unkhoff, M.; Frank, P.; Just, Th. *Proc. Combust. Inst.* **1989**, *22*, 1053−1061.
(32) Wu, C. H.; Singh, H. J.; Kern, R. D. *Int. J. Chem. Kinet.* **1987**, *19*, 975−996.
(33) Smith, S. C.; McEwan, M. J.; Gilbert, R. J. *J. Chem. Phys.* **1989**, *90*, 4265−4273.
(34) Ancia, R.; Vandooren, J.; Van Tiggelen, P. J. *Proc. Combust, Inst.* **1996**, *26*, 1009−1016.
(35) Kee, R. J.; Rupley, F. M.; Miller, J. A.; Coltrin, M. E.; Grcar, J. F.; Meeks, E.; Moffat, H. K.; Lutz, A. E.; Dixon-Lewis, G.; Smooke, M. D.; Warnatz, J.; Evans, G. H.; Larson, R. S.; Mitchell, R. E.; Petzold, L. R.; Reynolds, W. C.; Caracotsios, M.; Stewart, W. E.; Glarborg, P.; Wang, C.; Adigun, O.; Houf, W. G.; Chou, C. P.; Miller, S. F.; Ho, P.; Young, D. J. *CHEMKIN*, version 4.0, Reaction Design, Inc., San Diego, CA, 2004.
(36) Frenklach, M.; Clary, D. W.; Gardiner, W. C., Jr.; Stein, S. E. *Proc. Combust. Inst*. **1985**, *20*, 887−901.
(37) Frenklach, M.; Wang, H. In *Soot Formation in Combustion: Mechanisms and Models*; Bockhorn, H., Ed.; Springer-Verlag: Heidelberg, 1994; pp 165−190.
(38) Miller, J. A.; Klippenstein, S. J. *J. Phys. Chem. A* **2003**, *107*, 7783−7799.
(39) Fernandes, R. X.; Hippler, H.; Olzmann, M. *Proc. Combust. Inst.* **2005**, *30*, 1033−1038.
(40) Shafir, E. V.; Slagle, I. R.; Knyazev, V. D. *J. Phys. Chem. A* **2003**, *107*, 8893.
(41) Rasmussen, C. L.; Skoth-Rasmussen, M. S.; Jensen, A. D.; Glarborg, P. *Proc. Combust. Inst*. **2005**, *30*, 1023−1032.
(42) Klippenstein, S. J.; Miller, J. A. Unpublished results, 2004.
(43) Klippenstein, S. J.; Miller, J. A. The Reaction of n-C_4H_3 with Acetylene and the Dissociation of the Phenyl Radical, 2004, manuscript in preparation.